SANDSTONE SAMPLE CLASSIFICATION, USING HIGH RESOLUTION CT METHOD

Dohnalik M., Zalewska J., Kaczmarczyk J.
Oil and Gas Institute, Krakow, Poland

ABSTRACT

Pore scale imaging is a problem being investigated for many years. Most imaging methods result in 2D images obtained by optical or electron microscopy. The only way to obtain 3D pore structure information, using such methods, is image interpolation, which results with inaccuracies and uncertainties inherent in interpolation methods. Since microtomography has been implemented into geological surveys, it is possible to obtain very realistic spatial images of pore structure.

This work shows a method of sandstone sample classification. Binarized spatial images were analyzed and allowed to obtain a lot of information referring to pore structure like: sample porosity, pore volume, number of connected components, pore structure, tortuosity, and pore structure connectivity.

Next, images were segmented, basing on connected components volume, which were classified into 6 volume classes (the bigger a pore substructure, the higher the class). Then, each sample was analyzed referring to the volume class's participation in the whole samples' pore structure.

Based on pore substructure component volume and number, we could classify sandstone samples into 3 porosity types, where each type was characterized by different quantitative and qualitative pore structure characteristics.

Fluid flow simulation, with the use of finite elements method, was performed on the best reservoir properties sample.

INTRODUCTION

Porosity and permeability factors are the most demanded data for oil and gas industry. Computed microtomograhy was implemented [11] to geology as high emphasis was put to obtain new kind of information on rock pore structures and how hydrocarbons would behave in reservoir formations.

There are methods which give precise information regarding participation of pores of certain size [3,9]. The disadvantage is that the sample is useless for further investigations or it requires a hazardous agent (mercury porosimetry) to perform tests. Since X-ray computed microtomography (micro-CT) has been applied to rock sample analysis, it is possible to obtain well detailed information regarding pore structure, without using any chemical agents or sample destruction [4].

There are many papers [2] referring to pure (>95% of quartz) sandstone sample analysis (Fontainebleau, Berea). It is also possible to calculate sample permeability [1] and create pore structure models to perform numerical simulations that can allow to obtain such petrophysical properties as electrical properties [8], wetting effects, two phase flow and mercury injection capillary pressure.

The innovative aspect of this work is that it refers to the samples cored from sandstone rock formations that are very common in Polish oil and gas explorations.

The aim of this work was to analyze pore structure of rotliegend sandstone samples by interpretation of data obtained by micro-CT. Image processing allowed to obtain many data referring to sample porosity: pore substructure volume, number of connected pores, pore structure tortuosity and connectivity, and pore distribution irregularity.

In this paper, authors were focused on qualitative and quantitative information obtained by 3D image description and analysis. This led to classify analyzed samples into 3 groups, with significant differences in pore structures. Fluid flow simulation was performed on the best properties sample.

METHODS

Data acquisition

An X-tek (Nikon) Benchtop CT 160Xi system was used for testing. Scans were performed with 110 kV voltage and 74 µA current. Spot size was 6 µm (checked with JIMA x-ray resolution chart). The samples being examined were sandstone rocks cored to cylindrical shape, with the diameter of 1 cm. A Varian Paxscan 2520V flat panel detector, with the pixel size of 127×127 µm^2, was used, and the geometrical magnification was 22×. To avoid beam hardening artifact [7], a Cu filter was used (0.4 mm thickness), as well as a scanning algorithm to minimize ring artifacts. The isotropic voxel size of reconstructed images was $(5.8 \, \mu m)^3$.

Data processing

Reconstructed images were binarized, with the method of thresholding along boundaries [5]. The volume of each image was cropped to $1000 \times 1000 \times 400$ voxels to simplify computer operations for pore structure analysis.

Further computational procedure was as follows: total porosity was calculated according to formula (1):

$$\phi = \frac{V_p}{V_p + V_f} \qquad\qquad\qquad (1)$$

where V_p – volume of voxels assigned to pore phase and V_f – volume of voxels assigned to rock phase.

The number and volume of connected components called the subtypes of pore structure were counted. The connected components were divided into 6 volume classes according to Figure 1. 3D images of the pore structure divided into volume classes were used for qualitative description of the samples' pore structure, where each class corresponded to a different color (gray value).

Volume [voxel]	1-9	10-99	100-999	1 000-9 999	10 000-99 999	>100 000
Volume [µm³]	$2 \cdot 10^2 - 2 \cdot 10^3$	$2 \cdot 10^3 - 2 \cdot 10^4$	$2 \cdot 10^4 - 2 \cdot 10^5$	$2 \cdot 10^5 - 2 \cdot 10^6$	$2 \cdot 10^6 - 2 \cdot 10^7$	$> 2 \cdot 10^7$
Class	I	II	III	IV	V	VI

Figure 1. Pore structure subtype volume classification.

That led to obtaining such information as: pore distribution irregularity, sedimentation structures' influence on porosity distribution and crack description (shape and width).
Samples were analyzed by the number of pore structure subtypes in each class and by the percentage participation of each volume class in the total pore structure volume.
The tortuosity factor computation of each sample pore structure was performed, with the use of MAVI software. The tortuosity value can be interpreted as a connectivity factor since it is calculated only when pore structure assures connection in any of X, Y or Z image directions.

Sample characteristics
The samples being analyzed were eolian rotliegend sandstone samples cored from boreholes located in the North Sudeten Monocline in Poland. The samples could be characterized as poor porosity (<13%) and low permeability samples (average <2mD). Their average mineral composition was: 70% of quartz, 10% of feldspar, 10% of clays, 5% of calcite.

Fluid flow simulations
Upon image processing, finite-element method fluid-flow simulations were performed on a selected sample. Steady-state flow of nitrogen was simulated in COMSOL Multiphysics 3.5a in Navier-Stokes physics. The geometry was imported as the STL surface generated on the basis of binarized CMT image. Model preparation was described elsewhere [5,6]. Sample permeability was calculated according to the equation [10]:

$$K_{N-S} = \frac{\frac{\Phi}{A} L_i \cdot \int_A u_i dA}{\frac{\nabla p}{\gamma}},$$ (2)

where Φ is sample's porosity L_i – the length of the sample in i direction, u_i – the fluid velocity in i direction, A – the area of fluid outlet in given direction, ∇p – the gradient of pressure and γ – the fluid weight unit.

RESULTS
Results led to distinguish three different sandstone types due to their pore structure characteristics. Minimum, maximum (vertical lines range) and average values of each class participation in each type of the samples were calculated as shown in Figure 2. As type C samples had very close participation values for each class, figure 2 c) does not include long vertical lines.
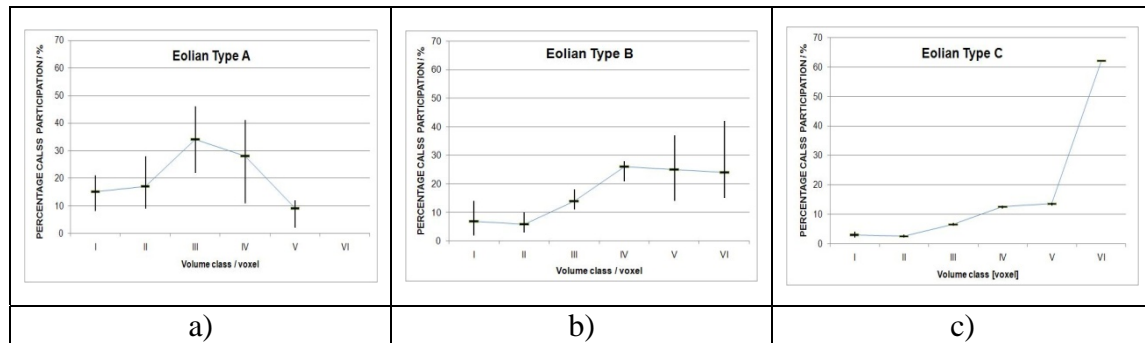
Figure 2. Each sample type's percentage volume classes participation.

The classification of rock types based on the cluster size corresponds to NMR results. Type A samples are on average 4,0 % of effective porosity, type B - 7,5% effective porosity and type C - 8,7% effective porosity. Figure 3 shows CT porosity versus mercury intrusion porosity values and shows, high pore space participation of small (micro) pores in type A samples.

Type A samples			Type B samples			Type C samples		
No.	Φ Hg/%	Φ CT/%	No.	Φ Hg/%	Φ CT/%	No.	Φ Hg/%	Φ CT/%
1	3,8	0,4	6	11,7	5,4	11	11,2	5,0
2	9,6	0,7	7	5,2	1,2	12	12,6	4,6
3	9,0	2,8	8	9,0	3,5			
4	7,0	1,5	9	10,5	4,8			
5	7,3	0,8	10	12,3	5,0			

Figure 3. micro-CT (Φ CT) and mercury intrusion (Φ Hg) porosity values.

Each of these samples' types can be characterized as follows:

Type A (5 samples): the samples with poor reservoir properties. The samples' total porosity was below 10%. In the majority of samples, pore structure regular distribution was observed (Figure 4a). As presented in Figures 2a, III and IV, volume classes dominated. All those samples had no VI volume class, and were characterized by high participation of small classes.

Type B (5 samples): the samples which may probably occur as good reservoir samples, but that cannot be definitely said based only on micro-CT images analysis. The samples' total porosity was more than 10%, some samples showed sedimentation structures influence on pore structure distribution irregularity (Figure 4b). As presented in Figures 2b, IV and V, volume classes dominated. The samples showed high participation of class VI and low participation of small classes.

Type C (2 samples): the samples with very good reservoir properties and with porosity higher than 10%. Volume class VI definitely dominates in both samples (Figure 2c). As shown in Figure 4c, the first sample had a very well developed pore structure, while the second one had an opened crack. Tortuosity analyses of those samples were possible. Pore structure connection occurs in two (2nd sample) or three (1st sample) directions.

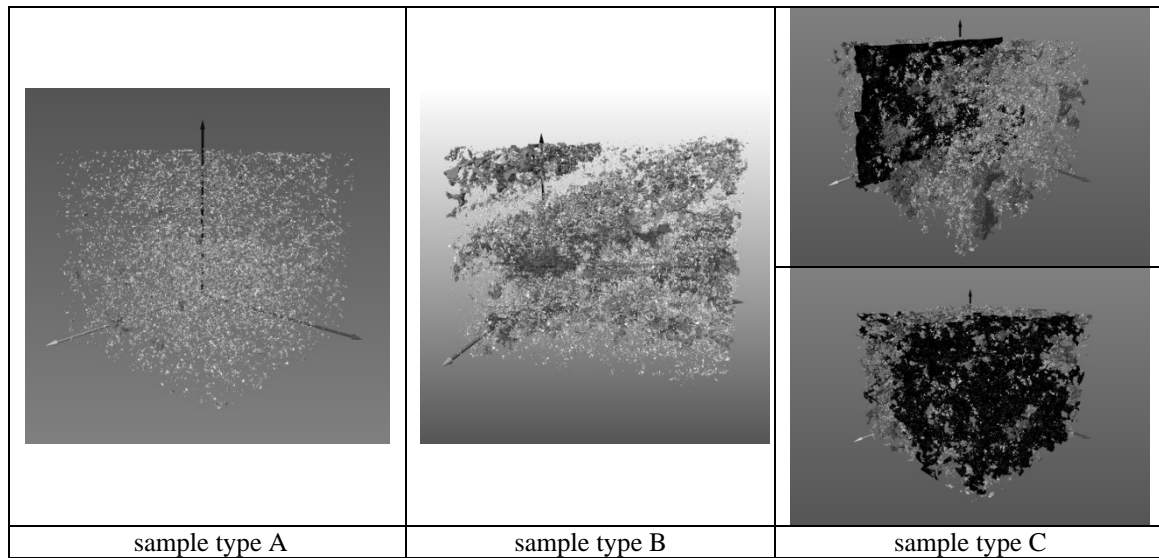| sample type A | sample type B | sample type C |

Figure 4. The most characteristic images of each of the sample types.

<u>Permeability simulations</u>

For the purpose of fluid flow simulation, crack from one of C-type samples was extracted. Binarized image was downsampled by factor 10 with the use of "majority wins" algorithm. Voxels were grouped into blocks 10x10x10. Then every group was substituted by a new voxels with the gray value of 1 (if most voxels in group were assigned to pores) or 0 (if the group was composed in most of rock layer). Next, to preserve pore system topology, the dilatation filter was used.

Fluid inputs and outputs were situated at the opposite sites of the crack. Permeability calculations (2) were consistent with gas permeability tests: measured permeability (K_{exp}) was 4.1 mD and the permeability evaluated from simulation data (k_{N-S}) was 7.1 mD. However, the relative error (difference between experimental and simulated value) of permeability estimation is high (73%), the difference of 3 mD is acceptable for an oil industry reservoir rock analysis. This error is due to a high downsampling factor during the image processing.

CONCLUSIONS

Internal rock pore structure analysis led to obtain some parameters regarding sample porosity, pore structure distribution, number of connected components, volume classified connected components and pore structure connectivity.

Due to low image resolution $(5.8 \ \mu m)^3$, it was not possible to use the results obtained as reference results because some information regarding macroporosity and all the information regarding microporosity was lost.

Based on the obtained results regarding volume classes participation and pore structure characteristics, eolian sandstone samples could be classified within 3 types (A, B or C).

Type A: the samples with poor reservoir properties.

Type B: the most difficult one to unambiguously describe as good reservoir samples. One has to keep in mind that, due to image resolution limitations, total porosity and

permeability will always be better than the results obtained with micro-CT as some pore connections are not considered in image analysis.

Type C: the samples of very good reservoir properties, where fluid-flow simulation was performed with high, but acceptable error.

REFERENCES

1. Arns C. H., Knackstedt M. A, Pinczewski W.V., Martys N.S., "Virtual permeametry on microtomographic images", *Journal of Petroleum Science and Engineering,* (2004) **45**, 1-2, 41– 46.
2. Arns J.Y., Sheppard A. P., Arns C. H., Knackstedt M. A., Yelkhovsky A., Pinczewski W.V., "Pore-level validation of representative pore networks obtained from micro-ctimages" International Symposium of the Society of Core Analysts (2007), Canada, paper SCA 2007-15
3. Cather M.E., Morrow N.R., Klich I., "Characterization of Porosity and Pore Quality in Sedimentary Rocks", *Studies in Surface Science and Catalysis*, (1991) **62**, 727-736
4. Cnudde V., Cwirzen A., Masschaele B., Jacobs P.J.S., "Porosity and microstructure characterization of building stones and concretes", *Engineering Geology*, (2009) **103,** 3-4, 76-83
5. Kaczmarczyk J., Dohnalik M., Zalewska J., V. Cnudde, The interpretation of X-ray Computed Microtomography images of rocks as an application of volume image processing and analysis, WSCG2010 Communication Paper Proceedings, pp. 23-30 (2010)
6. Kaczmarczyk J., Dohnalik M., Zalewska J., "Three-dimensional pore scale fluid flow simulation based on computed microtomography carbonate rocks' images", in proceedings: V European Conference on Computational Fluid Dynamics ECCOMAS CFD 2010 (2010, in press).
7. Ketcham R.A., Carlson W.D., "Acquisition, optimization and interpretation of X-ray computed tomographic imagery: applications to the geosciences", *Computers & Geosciences*, (2001) **27**, 381-400
8. Knackstedt M. A., Arns C. H., Sheppard A. P., Senden T. J., Sok R. M., Cinar Y., Olafuyi A. O., Pinczewski W. V., Padhy G., Ioannidis M., "Pore scale analysis of electrical resistivity in complex core material", International Symposium of the Society of Core Analysts (2007), Canada, paper SCA 2007-33
9. Masalmeh S.K., Jing X.D., "Capillary pressure characteristics of carbonate reservoirs: relationship betweendrainage and imbibition curves", International Symposium of the Society of Core Analysts (2006) Norway, paper SCA 2006-16
10. Narsilio G., Buzzi O., Fityus S., Yun T., Smith D., Upscaling of Navier-Stokes equations in porous media: Theoretical, numerical and experimental approach, Comput. Geotech. 36, iss. 7, pp. 1200-1206 (2009)
11. Van Geet M., Swennen R., Wevers M., "Quantitative analysis of reservoir rocks by microfocus X-ray computerised tomography", *Sedimentary Geology*, (2000) **132**, 1-2, 25-36